

Exploiting magnetic properties of Fe doping in zirconia^{*}

From first-principles simulations to the experimental growth and characterization of thin films

Davide Sangalli^{1,a}, Elena Cianci¹, Alessio Lamperti¹, Roberta Ciprian¹, Franca Albertini², Francesca Casoli², Pierpaolo Lupo², Lucia Nasi², Marco Campanini², and Alberto Debernardi¹

¹ Laboratorio MDM - IMM - CNR via C. Olivetti, 2 20864 Agrate Brianza (MB), Italy

² IMEM-CNR, Parco delle Scienze 37/A, 43124 Parma, Italy

Received 24 July 2012 / Received in final form 13 February 2013

Published online (Inserted Later) – © EDP Sciences, Società Italiana di Fisica, Springer-Verlag 2013

Abstract. In this study we explore, both from theoretical and experimental side, the effect of Fe doping in ZrO_2 ($\text{ZrO}_2\text{:Fe}$). By means of first principles simulation, we study the magnetization density and the magnetic interaction between Fe atoms. We also consider how this is affected by the presence of oxygen vacancies and compare our findings with models based on impurity band [J.M.D. Coey, M. Venkatesan, C.B. Fitzgerald, *Nat. Mater.* **4**, 173 (2005)] and carrier mediated magnetic interaction [T. Dietl, H. Ohno, F. Matsukura, J. Cibert, D. Ferrand, *Science* **287**, 1019 (2000)]. Experimentally, thin films (≈ 20 nm) of $\text{ZrO}_2\text{:Fe}$ at high doping concentration are grown by atomic layer deposition. We provide experimental evidence that Fe is uniformly distributed in the ZrO_2 by transmission electron microscopy and energy dispersive X-ray mapping, while X-ray diffraction evidences the presence of the fluorite crystal structure. Alternating gradient force magnetometer measurements show magnetic signal at room temperature, however, with low magnetic moment per atom. Results from experimental measures and theoretical simulations are compared.

1 Introduction

Dilute magnetic semiconductors (DMS) are materials in which magnetic impurities are introduced in order to produce a magnetic ground state. These systems have received great attention in recent years, since the discovery of carrier induced ferromagnetism in $(\text{In}, \text{Mn})\text{As}$ [1] and $(\text{Ga}, \text{Mn})\text{As}$ [2], and are believed to be fundamental to fabricate spin-based electronic devices. Recently, a new class of DMS has been investigated, namely DMS based on high- k oxides, i.e. dilute magnetic oxides (DMO), after the experimental evidence of room temperature magnetism in transition metals (TMs) doped zirconia [3–6] (ZrO_2), hafnia [7,8] (HfO_2), and titania [9,10] (TiO_2) and the theoretical prediction of high T_c in TMs doped ZrO_2 [11,12].

The understanding of DMS/DMO physical properties constitutes a challenge for the theory as the fundamental mechanism leading to ferromagnetic (FM) interaction between the dopants cannot be explained in terms of simple exchange mechanisms, at least at low doping concentration, being the latter often too short-ranged. Among the other, two theoretical models have been proposed to describe FM effects: the first is based on the presence

of impurity states in the crystal, impurity band model (IBM) [13], the other on carriers in spin polarized bands, carrier mediated model (CMM) [14] which is indeed a refined version of the Zener model.

From the experimental side the inclusion and influence of magnetic dopant, such as Fe, Co, Ni and Mn, is not clearly understood. Indeed, while several DMS/DMO have been predicted to have a Curie temperature (T_c) above room temperature, no experimental report of $T_c > 300$ K has been left unchallenged by other studies [15]. Moreover, some results suggest that magnetic impurities act as paramagnetic (PM) centers with unusually long relaxation time [16], at least at very low doping concentrations.

In this manuscript, we study iron doped zirconia ($\text{ZrO}_2\text{:Fe}$) focusing our attention on the magnetic properties of the system. In Section 2, we provide a structural characterization of thin films grown by atomic layer deposition (ALD). In particular, we show that the doping is uniform, with high iron concentration and no segregation, and that zirconia is in the tetragonal/cubic structure. Thus, theoretically, we focus our attention on the tetragonal structure of zirconia with substitutional iron doping uniformly distributed in the sample. In Section 3, we study the magnetization of the system and how it is influenced by defects, i.e. oxygen vacancies ($V_{\text{O}}^{\bullet\bullet}$), comparing our results with the IBM and the CMM. Indeed, in a recent work, we showed that iron doping induces $V_{\text{O}}^{\bullet\bullet}$, with a ratio $y_{V_{\text{O}}^{\bullet\bullet}}/Fe = 0.5$, for charge compensation, and

^{*} Contribution to the Topical Issue “New Trends in Magnetism and Magnetic Materials”, edited by Francesca Casoli, Massimo Solzi and Paola Tiberto.

^a e-mail: davide.sangalli@gmail.com

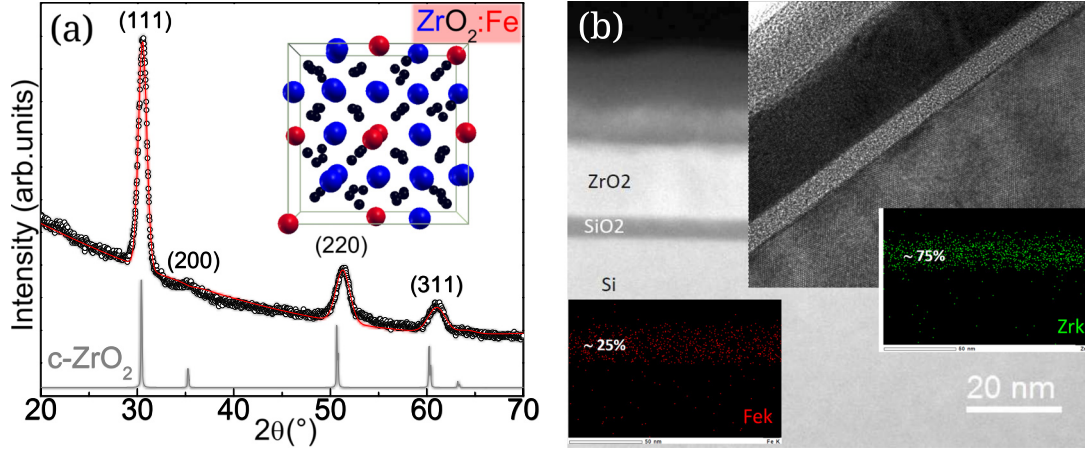


Fig. 1. Structural properties of iron doped zirconia. (a): XRD patterns show that the film presents the cubic/tetragonal phase [28]. A representation of the fully relaxed theoretical structure is also pictured with Fe atoms in red, Zr atoms in blue and oxygens in black (we used the Xcrysden software [29]). (b): HAADF image and HREM inset showing the layered geometry of the sample. The EDX chemical maps show a uniform doping distribution with no segregation.

that $\text{ZrO}_2\text{:Fe}$ films growth by ALD presents a ratio close to one half [17]. We finally investigate the magnetization of the films growth by ALD. From the magnetization at saturation, we extract the magnetic moment per atom which is discussed in view of the results from theoretical simulations.

2 Structural properties of $\text{ZrO}_2\text{:Fe}$

In order to describe the effect of iron doping in zirconia, $\text{ZrO}_2\text{:Fe}$ thin films were grown on Si/SiO₂ substrates in a flow-type hot wall atomic layer deposition reactor (ASM F120) starting from β -diketonates metalorganic precursors. Ozone was used as oxidizing gas in the reaction process. The Fe concentration in $\text{ZrO}_2\text{:Fe}$ films can be tuned tailoring the Zr/Fe precursors pulsing ratio. In the present work, however, we focused our attention on the high doping regime keeping the pulsing ratio fixed. The growth temperature was maintained at 350 °C. After the deposition the films were annealed at 600 °C in N₂ flux for 60 s to study their thermal stability. Further details on the samples preparation can be found in reference [18].

Film crystallinity was checked by X-ray diffraction (XRD) at fixed grazing incidence angle $\omega = 1^\circ$ and using Cu K α ($\lambda = 0.154$ nm) monochromated and collimated X-ray beam (Italstructure XRD 3000, details on the measurements can be found in Ref. [19]). In the present work, all measures shown are from the same film which we chose as representative of the high-doping concentration samples. Figure 1a shows that the films present a cubic/tetragonal crystalline structure with an estimated cell parameter, assuming a cubic cell, $a = 5.024$ Å with a contraction of about $(a_{\text{exp}} - a_{\text{theo}}^0)/a_{\text{theo}}^0 \approx -1.0\%$; here $a_{\text{exp}}^0 = 5.074$ is the lattice parameter measured for undoped ZrO_2 films. Theoretically, we found, at $x = 25\%$, $(a_{\text{theo}} - a_{\text{theo}}^0)/a_{\text{theo}}^0 \approx -0.4\%$, with $a_{\text{theo}}^0 = 5.11$, the lattice parameter computed for ZrO_2 , while the tetragonal deformation reduces from 3.05% to <1.0%.

The samples were then characterized by transmission electron microscopy (TEM), performed by a JEOL 2200FS microscope equipped with a high-angle annular-dark-field (HAADF) detector, in-column energy filter and energy dispersive X-ray (EDX) spectrometer. The layered geometry of the samples is shown in Figure 1b. The Fe atomic concentration measured by EDX is 25%, in agreement within few percent to the estimation done by X-ray photo-emission (XPS). The EDX maps, taken in different regions of the samples, showed that Fe is uniformly distributed across the film and no clusters or segregation at the grain boundaries have been found (see Fig. 1b, insets).

Thus, theoretically, we computed, from first-principles, the ground state of the tetragonal phase of $\text{ZrO}_2\text{:Fe}$ with uniform iron doping distribution. We used the PWSCF [20] package considering a super-cell with 96 atoms; for all systems the atomic positions are fully relaxed¹. The ground state was computed with the generalized gradient approximation [21] (GGA) to the density functional theory (DFT) scheme [22,23] with ultra-soft pseudo-potentials [24,25]. We have, recently, shown that iron, in the zirconia host lattice, behaves like Yttrium (Y), which is among the most studied dopant of this oxide: it replaces zirconium atoms in the ZrO_2 lattice inducing $V_{\text{O}}^{\bullet\bullet}$ for charge compensation, with a ratio $y_{V_{\text{O}}^{\bullet\bullet}/\text{Fe}} = 0.5$, and stabilizes the tetragonal phase above $x_{\text{Fe}} \approx 11\%$ [17,26]. Calculations have been done at different doping concentrations, $x_{\text{Fe}} = 6.24, 12.5, 25.0\%$ and different $V_{\text{O}}^{\bullet\bullet}$ concentration, considering the $V_{\text{O}}^{\bullet\bullet}$ to Fe ratios $y_{V_{\text{O}}^{\bullet\bullet}/\text{Fe}} = 0, 0.5, 1$, focusing our attention at the high doping concentration limit, i.e. the concentration measured experimentally. In the inset of Figure 1b, a relaxed structure at $y_{V_{\text{O}}^{\bullet\bullet}/\text{Fe}} = 0.5$ and $x_{\text{Fe}} = 25\%$, which is the expected structure in our films [17], is shown.

¹ We use a cut-off of 35 Ry for the wavefunctions and 400 Ry for the augmentation density; a Monkhorst-Pack grid $2 \times 2 \times 2$ for the Brillouin zone.

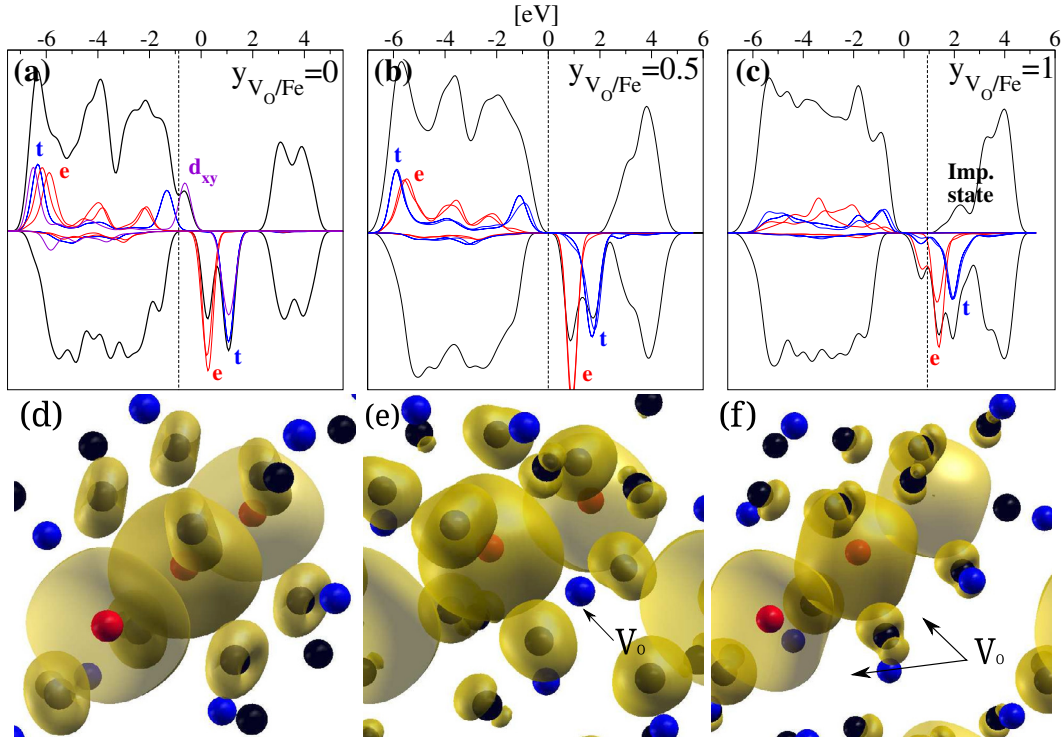


Fig. 2. (a–c) Theoretical density of states and (d–f) magnetization density isosurfaces at $m = 0.01$ a.u. for the ferromagnetic configuration at $y_{V_O^{2+}/Fe} = 0, 0.5, 1$. The density of states projected on the d atomic orbitals is also shown. The crystal field splitting is visible with the e doublet, d_{z^2} and $d_{x^2-y^2}$ in blue, at higher (lower) energy in the majority (minority) spin channel respect to the t triplet, d_{xy} , d_{xz} and d_{yz} in red. In panels d–f, Fe atoms are represented in red, Zr atoms in blue and oxygens in black.

In the next section, we discuss in details how the magnetic properties of the system and its electronic structure are correlated. In particular, the density of states (DOS) at the Fermi level can crucially affect the exchange mechanisms in the system. The results presented here are obtained within the GGA approximation which is known however, to suffer of the self-interaction problem and thus to de-localize too much the d electrons. Thus, the so-called Hubbard U parameter (GG + U scheme) is often used. Indeed in reference [17], we have discussed how this correction modify the DOS of the system. However, we have also shown that the $U = 0.0$ eV choice better reproduces the experimentally measured band structure. Accordingly, in the present manuscript, we discuss the magnetic properties in this configuration, i.e. within the simple GGA scheme, pointing out how the Hubbard U correction would eventually modify the conclusions of our approach.

3 Magnetic properties of $ZrO_2:Fe$

Starting from the fully relaxed structures considered at $x_{Fe} = 25\%$, we computed the local magnetization of the system. In Figure 2, the magnetization density, i.e. the difference between the spin-majority and the spin-minority density is represented for $y_{V_O^{2+}/Fe} = 0, 0.5, 1$. In order to compare the present results with the IBM, also the

total DOS are plotted. The FM configuration is considered for better clarity as it helps to distinguish between the minority and the majority spin channel. However, all the conclusion we will draw in the following also hold for the anti-FM configuration (see Figs. 3b and 3c for a comparison of the anti-FM magnetization density).

At $y_{V_O^{2+}/Fe} = 0$, the system shows holes in the valence band (Fig. 2a) because iron acts as an acceptor; the projected DOS shows that these are localized on the Fe (d_{xy}) level. As a consequence the majority-spin d band is not completely filled, the magnetic moment per iron atom is $4\mu_B$ and iron is forced in a +4 oxidation state. This also breaks the spherical symmetry of the system and the shape of the magnetization density close to the oxygens is not isotropic, with a peculiar doughnut shape oriented in the xy -plane.

Creating V_O^{2+} , i.e. increasing $y_{V_O^{2+}/Fe} > 0$, electrons are released in the system. These fill the empty d_{xy} levels with a charge-transfer mechanism. At $y_{V_O^{2+}/Fe} = 0.5$, the majority d band is completely filled, the magnetic moment per iron atom is $5\mu_B$ and the magnetization has a spherical shape. The system turns into a charge-transfer semi-conductor (Fig. 2b). At $y_{V_O^{2+}/Fe} = 1$, electrons fill the minority d levels and the magnetic moment per iron atom is reduced to $4\mu_B$. However, the minority d electron does not participate in the bonds, thus the anisotropy is only weakly transferred to the p orbitals of oxygen (Fig. 2c).

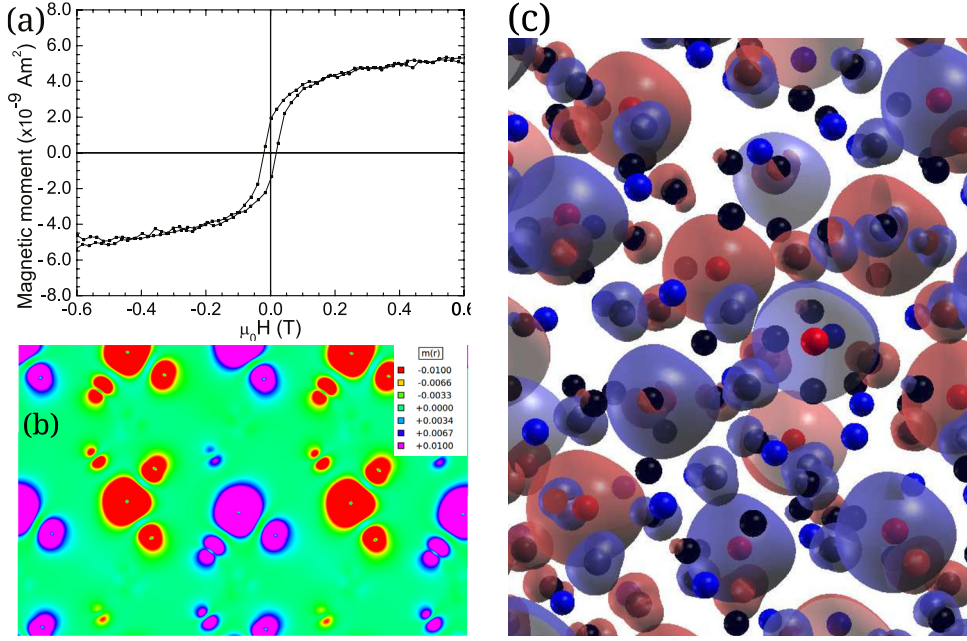


Fig. 3. (a) Magnetization hysteresis loop measured by alternating gradient force magnetometer at room temperature. The resulting magnetization at saturation can be interpreted in terms of an anti-ferromagnetic structure if $y_{V_{O}^{\bullet\bullet}/Fe}$ deviates from 0.5 of about 10%. The magnetization density for the anti-FM configuration at $y_{V_{O}^{\bullet\bullet}/Fe} = 0.5$ is plotted in panels (b–c). (b) 2D contour plot of the magnetization density along the plane (1 -1 0). (c) Positive (red) and negative (blue) isosurfaces of the magnetization density at $m = \pm 0.02$.

In all configurations, the magnetization is mainly located around the Fe atoms and it is in part transferred to the oxygen next nearest neighbor suggesting a short range magnetic interaction (Figs. 2d–2f).

It is worth to compare the DOS of our system with the IBM. A crucial assumption of the IBM is that the presence of $V_{O}^{\bullet\bullet}$ creates impurity states with poorly localized electrons. These, already at low doping concentration, would overlap to create an impurity band that can mediate the FM interaction among nearby iron atoms. Indeed $V_{O}^{\bullet\bullet}$ are a common defect in pure ZrO_2 films where they create impurity states close to the conduction band. However in the case for $\text{ZrO}_2:\text{Fe}$ the situation is different, as shown in Figures 2a–2c. For low $V_{O}^{\bullet\bullet}$ concentration, i.e. $y_{V_{O}^{\bullet\bullet}/Fe} \leq 0.5$ no impurity states are associated to $V_{O}^{\bullet\bullet}$ while for $x > 0.5$ impurity states appear but higher in energy than the empty spin minority d -levels. Thus the extra electrons are trapped in the Fe(d) levels and the impurity states remain empty. More in general, the majority of magnetic transition metals (TMs), i.e. Fe, Co, Ni, Mn, and Cr, have +2 or +3 as most stable oxidation state and we expect a similar picture for all TMs doped XO_2 oxides, at least for $y_{V_{O}^{\bullet\bullet}/Fe} \leq 0.5$ (1.0), in the case of +3 (+2) oxidation state. Thus, according to our results, the IBM cannot be invoked to describe the magnetic ground-state for $\text{ZrO}_2:\text{Fe}$ and for $\text{XO}_2:\text{TM}$ in general.

The situation depicted is much closer to the CMM proposed for $\text{Ga}_{1-x}\text{Mn}_x\text{As}$. In $\text{Ga}_{1-x}\text{Mn}_x\text{As}$, Mn acts as an acceptor which compensates the anti-site defects commonly present in GaAs giving a charge-transfer semiconductor; in $\text{ZrO}_2:\text{Fe}$, Fe acts as an acceptor compensating

the $V_{O}^{\bullet\bullet}$. The main difference between the two systems is the nature of the host lattice, a covalent semiconductor the former and a polar oxide the latter. In $\text{Ga}_{1-x}\text{Mn}_x\text{As}$, when x_{Mn} exceeds the anti site defect concentration, the system behaves like a metal with holes in the valence band. In $\text{ZrO}_2:\text{Fe}$ instead, at $y_{V_{O}^{\bullet\bullet}/Fe} < 0.5$, the holes are localized onto the d_{xy} states (see Fig. 2b); conduction could be possibly obtained only at high doping concentration with a hopping like mechanism.

The main effect of the Hubbard U term is to shift down in energy the occupied d orbitals. In particular, at $y_{V_{O}^{\bullet\bullet}/Fe} = 0$, this tends to de-localize the hole in the valence band from the iron d orbitals to the oxygen p levels. At $y_{V_{O}^{\bullet\bullet}/Fe} = 0.5$ no other qualitative change in the DOS can be observed. Finally, at $y_{V_{O}^{\bullet\bullet}/Fe} = 1$, the Hubbard U correction opens a gap between the occupied and the empty d orbitals in the minority spin channel. However, all the consideration on the IBM and the CMM still holds. The de-localization of the holes for $y_{V_{O}^{\bullet\bullet}/Fe} < 0.5$ could possibly make the system more similar to standard DMS as $\text{Ga}_{1-x}\text{Mn}_x\text{As}$. However, we remind that in the case of $\text{ZrO}_2:\text{Fe}$, the Hubbard U correction does not improve the description of the electronic properties of the system over standard GGA [17]. Also, the de-localization of holes in oxides is under debate [27].

We then focus our attention on the strength of the magnetic interaction in our system. This in principle can be understood computing the energy difference between the FM and the PM phase. The latter however can be hardly described within a periodic code, as the description

of random magnetic moment orientations would require huge super-cells with a non-collinear description of the wavefunctions. The energy difference per iron atom between the FM and the anti-FM configuration however can be used as a reasonable approximation [15]. We found that at lower doping, $x_{Fe} = 6.25$, 12.5%, the energy difference is very low with $\Delta E/k_B$ of the order of few Kelvin². The anti-FM configuration is slightly favored at $y_{V_O^{\bullet\bullet}/Fe} = 0.5$, while the FM one is slightly favored at $y_{V_O^{\bullet\bullet}/Fe} = 0$. Instead at $x_{Fe} = 25\%$, in both cases, the anti-FM configuration is favored with $\Delta E/k_B \approx 150$ K for $y_{V_O^{\bullet\bullet}/Fe} = 0.5$ and $\Delta E/k_B \approx 20$ K for $y_{V_O^{\bullet\bullet}/Fe} = 0$. This suggests a short range interaction which becomes relevant at $x_{Fe} > x_P$, with x_P the percolation threshold, i.e. an anti-FM super-exchange mechanism which is dominant in the $y_{V_O^{\bullet\bullet}/Fe} = 0.5$ case. For the $y_{V_O^{\bullet\bullet}/Fe} = 0$ configuration, however, this super-exchange mechanism appears to be in competition with a FM interaction which could be explained in terms of the CMM model, though with a weaker effect due to the low mobility of the holes. This results in a weakly FM interaction at low doping and a weakly anti-FM interaction at higher doping. In this case, the predictions of the GGA + U approach are substantially different. Indeed the U correction, de-localizing the holes, strongly enhances the CMM mechanism and indeed the systems turns out to be ferromagnetic at any doping concentration with $\Delta E/k_B \approx 150$ K at $x_{Fe} = 25\%$.

Experimentally, the magnetic properties of sample with $x_{Fe} \approx 25\%$ were studied by means of alternated gradient force magnetometry (AGFM). Magnetization measurements, performed at room temperature by applying the magnetic field parallel to the film plane, show a clear hysteresis loop characterized by a coercive field $\mu_0 H_c \approx 0.03$ T (Fig. 3a). From the saturation magnetization value a magnetic moment per Fe atom $m \approx 0.6\mu_B$ can be extrapolated. This is consistent with the values reported in the literature but is one tenth of the theoretically predicted value, $m \approx 5\mu_B$. Moreover, theoretically we found that the anti-FM configuration is the most stable at least for $y_{V_O^{\bullet\bullet}/Fe} = 0.5$, which is the expected situation in our films [17]. In Figures 3b and 3c, we plotted the magnetization density in the anti-FM configuration for $y_{V_O^{\bullet\bullet}/Fe} = 0.5$. As in the case of FM ground state, the magnetization is mainly located on the Fe atoms and the next nearest neighbor oxygens.

The discrepancy between the theoretically and the experimental results could be possibly explained supposing that experimentally $y_{V_O^{\bullet\bullet}/Fe} = 0.5$ were not fulfilled by few percent of the Fe atoms, which thus would be in the Fe^{4+}/Fe^{2+} oxidation state. If we assume that these ions would couple with FM interaction, with a CMM like mechanism, the net results would be a weak magnetic system with low magnetic moment per atom. Also in this case, however, the energy difference between the FM and the

anti-FM configuration is too low to explain the experimental result. A possible mechanism to explain the room temperature magnetism is suggested by the LDA + U approach where the de-localization of the holes strongly enhances the CMM mechanism. However, further investigations are needed, both experimentally and theoretically, to clarify this point.

4 Conclusions

In conclusion, we have studied both theoretically and experimentally thin films of iron doped ZrO_2 . Experimentally, we have shown that iron distributes uniformly at high doping concentration with no cluster formation and that the system is magnetic at room temperature. With first principles simulations we have discussed the possible magnetization mechanisms comparing our results with other model proposed in the literature. We showed that the impurity band model cannot be invoked in the case of iron doped zirconia while the carrier mediated model could be possibly considered for uncompensated oxygen vacancies concentration (i.e. $y_{V_O^{\bullet\bullet}/Fe} \neq 0.5$). The standard super-exchange mechanism however appears to be dominant for $y_{V_O^{\bullet\bullet}/Fe} = 0.5$.

From magnetization measurements of highly doped samples, we found a low saturation magnetization value corresponding to low magnetic moment per Fe atom. We tried to interpret the experimental results in view of our theoretical findings. However, the difference between theory and experiments suggest that other effects need to be taken into account for a correct description of the magnetic properties of the system. The role of the Hubbard U correction together with the deviation from the theoretically ideal $y_{V_O^{\bullet\bullet}/Fe} = 0.5$ configuration have been proposed as possible candidates.

This work was funded by the Cariplo Foundation through the OSEA project (No. 2009-2552). Helpful discussions with L. Lazzarini are gratefully acknowledged. D.S. and A.D. would like to acknowledge G. Onida and the ETSF Milan node for the opportunity of running simulations on the “etsfmi cluster”, and P. Salvestrini for technical support on the cluster. We also acknowledge computational resources provided by the Consorzio Interuniversitario per le Applicazioni di Supercalcolo Per Università e Ricerca (CASPUR) within the project MOSE.

References

1. H. Ohno, H. Munekata, T. Penny, S. Von Molnar, L.L. Chang, Phys. Rev. Lett. **68**, 2664 (1992)
2. H. Ohno, A. Shen, F. Matsukura, A. Oiwa, A. Endo, S. Katsumoto, Y. Iye, Phys. Rev. Lett. **69**, 363 (1996)
3. N.H. Hong, C.-K. Park, A.T. Raghavender, O. Ciftja, N.S. Bingham, M.H. Phan, H. Srikanth, J. Appl. Phys. **111**, 07C302 (2012)
4. J.M.D. Coey, M. Venkatesan, P. Stamenov, C.B. Fitzgerald, L.S. Dorneless, Phys. Rev. B **72**, 024450 (2005)

² The ferromagnetic structure at $x_{Fe} = 12.5\%$ is frustrated. Considering the closest Fe-Fe atoms we have in total, within in the supercell, 6 anti-ferromagnetic “connections” and 2 ferromagnetic connections.

5. T.R. Sahoo, S.S. Manoharan, S. Kurian, N.S. Gajhiye, *Hyperfine Interaction* **188**, 43 (2009)
6. V.V. Kriventsov, D.I. Kochubey, Y.V. Maximov, I.P. Suzdalev, M.V. Tsodikov, J.A. Navio, M.C. Hidalgo, G. Colón, *Nucl. Instrum. Meth. Phys. Res. A* **470**, 341 (2001)
7. N.H. Hong, J. Sakai, N. Poirot, A. Ruyter, *Appl. Phys. Lett.* **86**, 242505 (2005)
8. N.H. Hong, N. Poirotet, J. Sakai, *Appl. Phys. Lett.* **89**, 042503 (2006)
9. Y. Matsumoto et al., *Science* **291**, 854 (2001)
10. Z.J. Wang, K.J. Tang, L.D. Tung, W.L. Zhou, L. Spinu, *J. Appl. Phys.* **93**, 7870 (2003)
11. S. Ostanin, A. Ernst, L.M. Sandratskii, P. Bruno, M. Däne, I.D. Hughes, J.B. Staunton, W. Hergert, I. Mertig, J. Kudrnovský, *Phys. Rev. Lett.* **98**, 016101 (2007)
12. T. Archer, C.D. Pemmaraju, S. Sanvito, *J. Magn. Magn. Mater.* **316**, e188 (2007)
13. J.M.D. Coey, M. Venkatesan, C.B. Fitzgerald, *Nat. Mater.* **4**, 173 (2005)
14. T. Dietl, H. Ohno, F. Matsukura, J. Cibert, D. Ferrand, *Science* **287**, 1019 (2000)
15. K. Sato, L. Bergqvist, J. Kudrnovsky, P.H. Dederichs, O. Eriksson, I. Turek, B. Sanyal, G. Bouzerar, H. Katayama-Yoshida, V.A. Dinh, T. Fukushima, H. Kizaki, R. Zeller, *Rev. Mod. Phys.* **82**, 1633 (2010)
16. H.P. Gunnlaugsson, T.E. Mlholt, R. Mantovan, H. Masenda, D. Naidoo, W.B. Dlamini, R. Sielemann, K. Baruth-Ram, G. Weyer, K. Johnston, G. Langouche, S. Olafsson, H.P. Gislason, Y. Kobayashi, Y. Yoshida, M. Fanciulli, ISOLDE Collaboration, *Appl. Phys. Lett.* **97**, 142501 (2010)
17. D. Sangalli, E. Cianci, R. Ciprian, A. Lamperti, M. Perego, A. Debernardi, *Phys. Rev. B* **87**, 085206 (2013)
18. A. Lamperti, E. Cianci, R. Ciprian, D. Sangalli, A. Debernardi, *Thin Solid Films* **533**, 83 (2013)
19. A. Lamperti, L. Lamagna, G. Congedo, S. Spiga, *J. Electrochem. Soc.* **158**, G211 (2011)
20. P. Giannozzi, S. Baroni, N. Bonini, M. Calandra, R. Car, C. Cavazzoni, D. Ceresoli, G.L. Chiarotti, M. Cococcioni, I. Dabo, A. Dal Corso, S. Fabris, G. Fratesi, S. de Gironcoli, R. Gebauer, U. Gerstmann, C. Gougoussis, A. Kokalj, M. Lazzeri, L. Martin-Samos, N. Marzari, F. Mauri, R. Mazzarello, S. Paolini, A. Pasquarello, L. Paulatto, C. Sbraccia, S. Scandolo, G. Sclauzero, A.P. Seitsonen, A. Smogunov, P. Umari, R.M. Wentzcovitch, *J. Phys.: Condens. Matter* **21**, 395502 (2009), <http://www.quantum-espresso.org>
21. J.P. Perdew, K. Burke, M. Ernzerhof, *Phys. Rev. Lett.* **77**, 3865 (1996)
22. P. Hohenberg, W. Kohn, *Phys. Rev.* **136**, B864 (1964)
23. W. Kohn, L.J. Sham, *Phys. Rev.* **140**, A1133 (1965)
24. D. Vanderbilt, *Phys. Rev. B* **41**, 7892R (1990)
25. A.M. Rappe, K.M. Rabe, E. Kaxiras, J.D. Joannopoulos, *Phys. Rev. B* **41**, 1227R (1990)
26. D. Sangalli, A. Debernardi, *Phys. Rev. B* **84**, 214113 (2011)
27. J.B. Varley, A. Janotti, C. Franchini, C.G. Van de Walle, *Phys. Rev. B* **85**, 081109R (2012)
28. International Crystal Structure Database, FIZ Karlsruhe and NIST ed., Release 2010 Code #68589 (*t*-ZrO₂)
29. A. Kokalj, *Comp. Mater. Sci.* **28**, 155 (2003)